

Comparison and selection strategy among compensating topologies in two-coil resonant wireless power transfer systems

Ali Agcal*, Selin Ozcira Ozkilig** and Kemalettin Toraman***

*Department of Electrical and Electronics Engineering, Suleyman Demirel University, Isparta, 32260, Turkey

**Department of Electrical Engineering, Yildiz Technical University, Istanbul, 34220, Turkey.

***Baskale Vocational School, Van Yuzuncu Yil University, Van, 65080, Turkey

**Corresponding Author: sozcira@yildiz.edu.tr

Submitted : 16-05-2021

Revised : 28-12-2021

Accepted : 09-01-2022

ABSTRACT

In this study, different compensation topologies for two-coil resonant wireless power transfer systems were compared. Compensation circuits were examined individually according to system parameters such as efficiency, equivalent impedance, frequency, load resistance, and phase angle. System variables were compared to address the constraints on system applicability regarding compensation topology selection in Wireless Power Transfer (WPT) systems. The main motivation of this study is to present a suitable topology selection scheme and flow diagram based on applications with various voltages, currents, powers, and loads. Simulations carried out using Simulink for the four main topologies under various load conditions indicated that choosing the proper compensation topology for an appropriate load is essential. The simulation results were validated using both Matlab and C # calculation codes. Analyses according to frequency under various load conditions show that efficiency variations depend on the compensation topology of the receiver side. Furthermore, this study revealed that the topology of the transmitter side only affects the equivalent impedance and amount of power drawn from the input; hence, it has no effect on the efficiency and load characteristics. Consequently, for low-load resistance, such as electric vehicle or mobile phone charging, topologies with series compensation on the receiver side are preferred. Correlatively, topologies with parallel compensation on the receiver side can be evaluated as suitable for high-load resistance, low-current, and low-power operations, such as biomedical appliance charging.

Keywords: Series-Series Compensation; Series-Parallel Compensation; Parallel-Series Compensation; Parallel-Parallel Compensation; Wireless Power Transfer.

INTRODUCTION

A Wireless Power Transfer (WPT) system transfers electrical energy from one point to another through an air gap without direct electrical connections. Energy is transferred from the primary coil to the secondary coil via electromagnetic induction over the air gap. Owing to the lack of contact, this system has advantages such as ease of use, high safety, high reliability, low maintenance costs, and a long service life. This technology is used in applications such as electrical vehicles, consumer electronics, and biomedical applications where conventional wired systems are undesirable (Hasanzadeh and Vaez-Zadeh, 2015; Tang and Cheng, 2020; Keerthi et al., 2018). The basic principle of an electromagnetically coupled resonance-based WPT system is that two coils with the same resonant frequency can efficiently transfer energy (Agcal et al., 2016). Because the efficiency of inductive power transfer based on magnetic induction decreases as the airgap distance increases, its popularity has decreased in recent years, being replaced by electromagnetic resonance coupling (Nataraj et al., 2018; Zeng et al., 2021; Aydin et al., 2021; Bekiroglu et al., 2018; Heidarian and Burgess, 2020). When the distance between the primary and secondary coils is large, the coupling coefficient decreases. Therefore, it is necessary to operate at higher frequencies to provide the required power. For high-power applications, the operating frequency is limited to less than 100 kHz owing to switching losses. Additionally, the primary and secondary parts are enabled to operate in resonance to minimize the amount of energy drawn from the power source and increase the power transfer. There

are two major disadvantages in sizing/planning a system in magnetically coupled resonance theory, the first of which is the physical dimensions of the system. If the size of the secondary-side coil decreases, the magnetic flux of the primary-side coil decreases drastically. For the magnetic flux to transfer energy efficiently, a large current must flow through the primary-side coil (Heidarian and Burgess, 2020). The second disadvantage is the fact that as the frequency becomes higher, the impedance of the primary side becomes more inductive. Consequently, the power factor becomes extremely small and approaches zero as the frequency increases, leading to a higher VA rating and reduced efficiency. Four types of compensation circuit topologies are currently used (Agcal et al., 2016; Ravikiran and Keshri, 2017; Zavrel and Kindl, 2018). In this study, different compensation topologies WPT systems were compared and investigated. The main aim of this study is to address the constraints in system applicability regarding compensation topology selection in WPT systems. Compensation circuits were examined individually with respect to system parameters such as efficiency, equivalent impedance, frequency, load resistance, and phase angle. The simulations performed in this study for four different topologies under various load conditions showed that choosing the proper topology for an appropriate load is very important. Analyses according to frequency under different load conditions showed that the variation in efficiency depends on the topology of the receiver side. Moreover, this study revealed that the topology of the transmitter side only affects the equivalent impedance and amount of power drawn from the input; hence, it has no effect on the efficiency and load characteristics.

WPT SYSTEM AND BASIC COMPENSATION TOPOLOGIES

Magnetically coupled WPT is based on the principle of transferring energy from one side to another via a magnetic connection between the receiver and transmitter coils. A magnetically coupled WPT system without compensation is shown in Figure 1, where V_s is the voltage source, L_1 and L_2 are the self-inductances of both coils, respectively, R_1 and R_2 are the inner resistances of the transmitting and receiving coils, respectively, L_m is the mutual inductance between the two coils, and R_L is the load resistance. I_T and I_R are the currents of the transmitter and receiver, respectively.

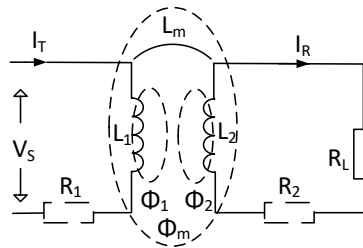


Figure 1 Magnetically coupled WPT system without compensation.

In this system, the power coefficient is very low because of the inductive effect of the coils. Therefore, compensation methods are used to make the power factor approach unity. In WPT systems, a single-layer spiral inductance with a high coupling effect between the receiver and the transmitter is generally preferred. The self-inductance of spiral inductance is calculated using Equation (1), and the mutual inductance expression is derived from the Neumann equation in Equation (2) (Waters et al., 2014; Gao et al., 2018).

$$L = \frac{N^2(D_0 - N(w+p))^2}{16D_0 + 28N(w+p)} \frac{39.37}{10^6} \quad (1)$$

where L : self-inductance; N : number of turns; D_0 : outer diameter; w : cable diameter; and p : spacing between turns. According to Equation (1), the single-layer spiral inductance self-inductance depends on the number of turns, outer coil diameter, cable diameter, and spacing between turns.

$$L_m = \frac{\mu_0 N_1 N_2}{4\pi} \oint_{l_1} \oint_{l_2} \frac{dl_1 dl_2}{r} \quad (2)$$

where N_1 and N_2 are the number of turns of the transmitter and receiver coils, respectively. The mutual inductance depends on the number of turns of the transmitter and receiver coils and on the geometric position at the axial and radial axes. Therefore, L and L_m are important circuit parameters affecting the efficiency and Z_{Eq} of a WPT system. In addition, the topologies formed according to how L and C are connected to the circuit determine the manner in which the WPT system works. In this paper, compensation circuit topologies are analyzed, and a topology selection scheme related to circuit parameters is presented. The SS topology circuit is illustrated in Fig 2.

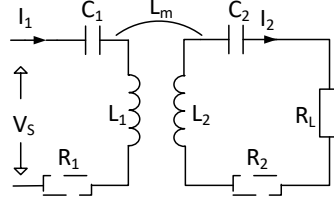


Figure 2 SS topology.

In the SS topology, the resonator capacitance of the transmitter and receiver capacitors are C_1 and C_2 , respectively. The equivalent impedance and efficiency formulations are shown in Equations (4) and (5), respectively. Z_{EqSS} is the equivalent impedance of the SS topology and η_{ss} is the efficiency of this system.

$$Z_{1,2} = R_{1,2} + j\omega L_{1,2} \quad (3)$$

$$Z_{EqSS} = Z_1 + \left(\frac{1}{j\omega C_1} \right) + \left(\frac{L_m^2 \omega^2}{Z_2 + \left(\frac{1}{j\omega C_2} \right) + R_L} \right) \quad (4)$$

$$\eta_{SS} = \left| \left(\frac{jL_m \omega}{Z_2 + \left(\frac{1}{j\omega C_2} \right) + R_L} \right)^2 \frac{R_L}{Z_{Eq}} \right| \quad (5)$$

The SS topology is more efficient at a low R_L ; therefore, the SP topology is preferred over the SS topology for systems with a higher R_L . The SP topology circuit is shown in Figure 3.

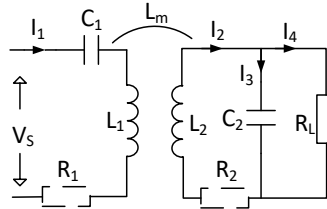


Figure 3 SP topology.

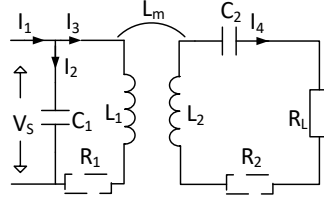
The equivalent impedance (Z_{EqSP}) and efficiency (η_{SP}) formulations of the SP topology are presented in Equations (7) and (8), respectively.

$$Z_L = R_L / (1 + j\omega C_2 R_L) \quad (6)$$

$$Z_{EqSP} = Z_1 + \frac{1}{j\omega C_1} + \frac{\omega^2 L_m^2}{Z_2 + Z_L} \quad (7)$$

$$\eta_{SP} = \left| R_L \left(\frac{j\omega L_m}{Z_2 + Z_L} \frac{1}{1 + j\omega C_2 R_L} \right)^2 / Z_{EqSP} \right| \quad (8)$$

The PS topology works efficiently at a low R_L with the same load range as the SS topology; however, unlike the SS topology, its equivalent impedance at the resonance frequency is much higher than that of the SS topology. The PS topology circuit is illustrated in Figure 4.

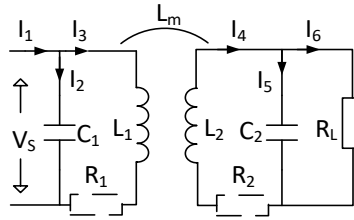

Figure 4 PS topology.

The equivalent impedance and efficiency of the PS topology, which are given in Equations (9) and (10), respectively, are derived from Figure 4, where Z_{EqPS} is the equivalent impedance of the PS topology and η_{PS} is the efficiency of this system.

$$Z_{EqPS} = \frac{Z_1 + \frac{\omega^2 L_m^2}{Z_2 + \frac{1}{j\omega C_2} + R_L}}{1 + j\omega C_1 \left(Z_1 + \frac{\omega^2 L_m^2}{Z_2 + \frac{1}{j\omega C_2} + R_L} \right)} \quad (9)$$

$$\eta_{PS} = \left| R_L \left(\frac{j\omega L_m}{Z_2 + \frac{1}{j\omega C_2} + R_L} \frac{\frac{1}{j\omega C_1}}{\frac{1}{j\omega C_1} + Z_1 + \frac{\omega^2 L_m^2}{Z_2 + \frac{1}{j\omega C_2} + R_L}} I_1 \right)^2 / Z_{EqPS} \right| \quad (10)$$

The PP topology, which has properties of the secondary side of the SP topology and the primary side of the PS topology, works efficiently at high loads and has a high equivalent impedance at the resonant frequency. The PP topology circuit is depicted in Figure 5.


Figure 5 PP topology.

The equivalent impedance and efficiency of the PP topology, which are given in Equations (11) and (12), respectively, are derived from Figure 5, where Z_{EqPP} is the equivalent impedance of the PP topology and η_{PP} is the efficiency of this system.

$$Z_{EqPP} = \frac{Z_1 + \frac{\omega^2 L_m^2}{Z_2 + Z_L}}{1 + j\omega C_1 \left(Z_1 + \frac{\omega^2 L_m^2}{Z_2 + Z_L} \right)} \quad (11)$$

$$\eta_{PP} = \left| R_L \left(\frac{1}{1 + j\omega C_2 R_L} \frac{j\omega L_m}{Z_2 + Z_L} \frac{\frac{1}{j\omega C_1}}{\frac{1}{j\omega C_1} + Z_1 + \frac{\omega^2 L_m^2}{Z_2 + Z_L}} I_1 \right)^2 / Z_{EqPP} \right| \quad (12)$$

$$Z_{EqPP}$$

SIMULATIONS FOR THE COMPARATIVE EVALUATION

The circuit parameters were determined to compare the efficiency and equivalent impedance of the four topologies under various load conditions. The WPT system parameters used in the simulations are listed in Table 1.

Table 1 Circuit parameters.

Parameter	Value
Transmitter inductance (L_1)	100 μ H
Receiver inductance (L_1)	100 μ H
Transmitter capacitance (C_1)	37 nF
Receiver capacitance (C_2)	37 nF
Transmitter Coil resistance (R_1)	0.2 Ω
Receiver Coil resistance (R_2)	0.2 Ω
Mutual inductance (L_m)	20 μ H

The variation in efficiency according to frequency under different load conditions is shown in Figure 6 using Equations (5), (8), (9), and (10) for the SS, SP, PS, and PP topologies, respectively. To examine the effects of different topologies on Z_{Eq} , the variation in the equivalent impedance under different load conditions is shown in Figure 7 using Equations (4), (7), (9), and (10).

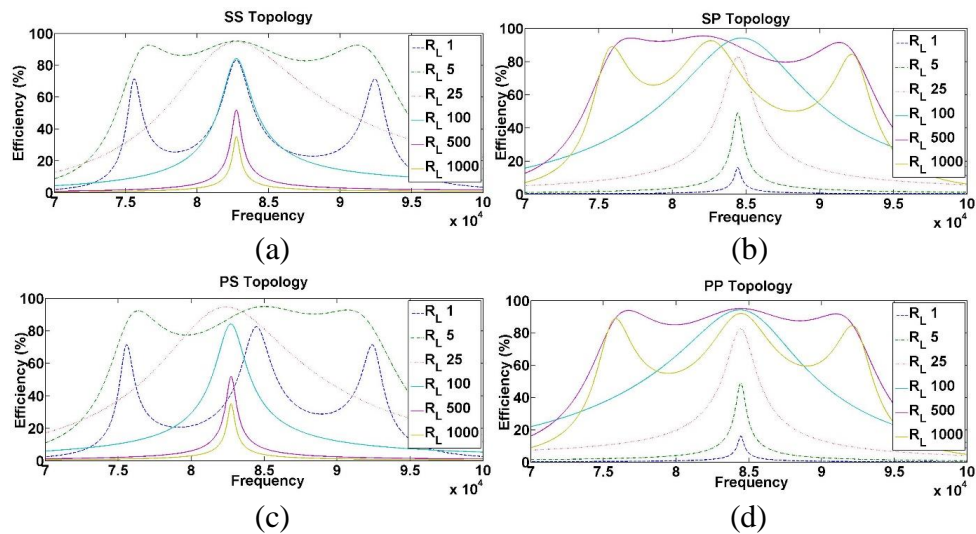


Figure 6 Efficiency-frequency graph for the (a) SS, (b) SP, (c) PS, and (d) PP topologies.

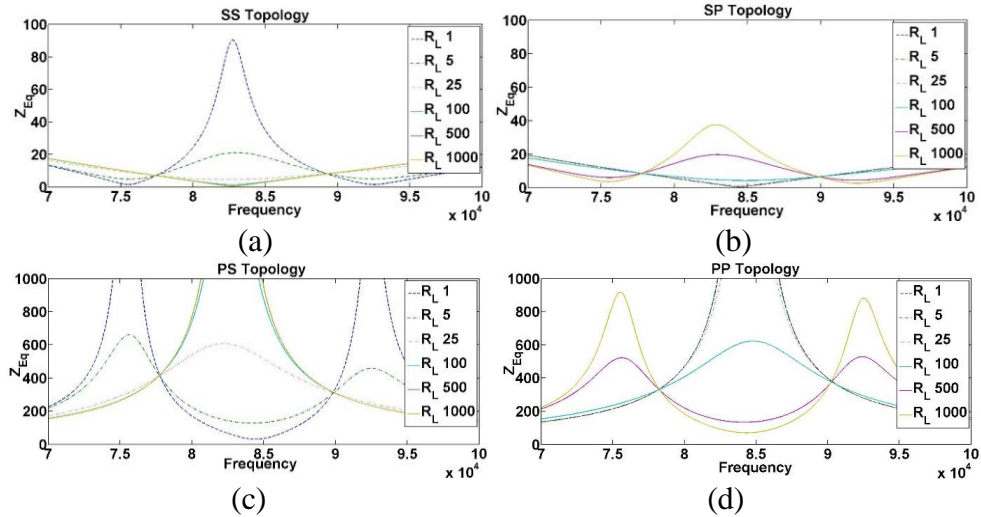


Figure 7 Equivalent impedance-frequency graph for the (a) SS, (b) SP, (c) PS, and (d) PP topologies.

In all four topologies, the efficiency of the energy transferred to the load resistance depends on the topology of the receiver side. When the results for all topologies are compared, it is revealed that the topologies with serial compensation on the receiver side exhibit a higher efficiency for low load resistances; therefore, the efficiency decreases as the load resistance increases, and vice versa. As the load resistance decreases below the critical value, a bifurcation phenomenon occurs. Despite the efficiency reaching its maximum, the resonance frequency bifurcates from one resonant frequency to three separate resonance frequencies. If the load resistance is lowered excessively, the efficiency starts to decrease, even in the bifurcation state, because the secondary side operates as a short circuit. However, the efficiency of the topologies with parallel compensation on the receiver side is higher, and the efficiency decreases as the load resistance decreases, and vice versa. In a parallel topology, the frequency bifurcates when the value of the load resistance increases above the critical value. In this range, the efficiency was at its maximum; however, there were three resonance frequencies. If the load resistance increases significantly, the efficiency decreases again in the region of the three resonance frequencies because the secondary side starts working as an open circuit.

Figure 7 shows that the compensation topology of the transmitter side in the SS, SP, PS, and PP topologies determines the equivalent impedance range at the resonant frequency. Figures 7 (a) and (b) reveal that the SS and SP topologies operate at a low equivalent impedance, whereas Figures 7 (c) and (d) reveal that the PS and PP topologies operate at a high equivalent impedance. In WPT systems, for topologies with serial compensation on the transmitter side, the resonance frequency becomes the frequency at which the equivalent impedance value is minimized. In the case of topologies with parallel compensation on the transmitter side, the resonance frequency becomes the frequency at which the equivalent impedance is maximized. At the resonance frequency, the equivalent impedance of the series topologies is low (1–10 Ω), while the equivalent impedance is high (100–10 k Ω) in the parallel topologies. Therefore, when both compensation topologies are supplied by a constant-voltage AC source, the serial-compensated topology draws more power from the AC source than the parallel-compensated topology. In terms of the amount of current drawn, the effect of the load resistance on efficiency should be investigated. Figure 8 shows the change in efficiency according to the load resistance for the SS and PS topologies.

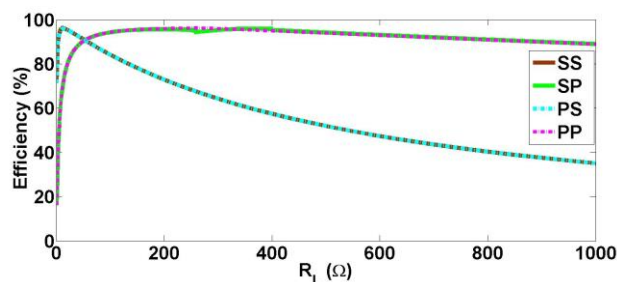


Figure 8 Efficiency-load resistance graph for the SS, SP, PS, and PP topologies.

Figure 9 shows that topologies with the same compensation on the receiver side have the same efficiency-load characteristics. To observe the transition between the capacitive and inductive operation points, which is essential to avoid the power factor becoming smaller, the change in phase angle with respect to frequency should also be investigated.

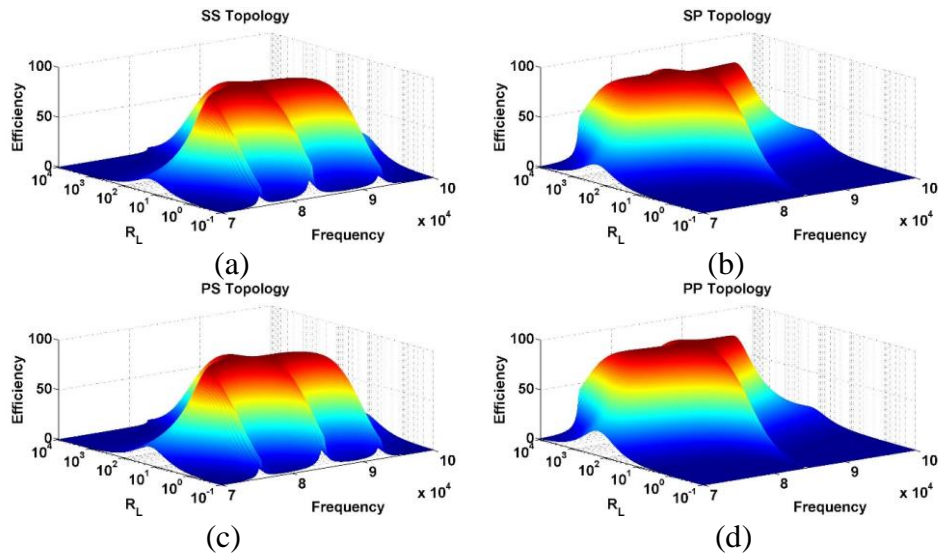


Figure 9 Efficiency-load resistance-frequency graphs for the (a) SS, (b) SP, (c) PS, and (d) PP topologies.

As shown in Figure 10, when the variation in phase angle for the four topologies according to frequency is examined, the phase angles are zero at the resonance frequencies.

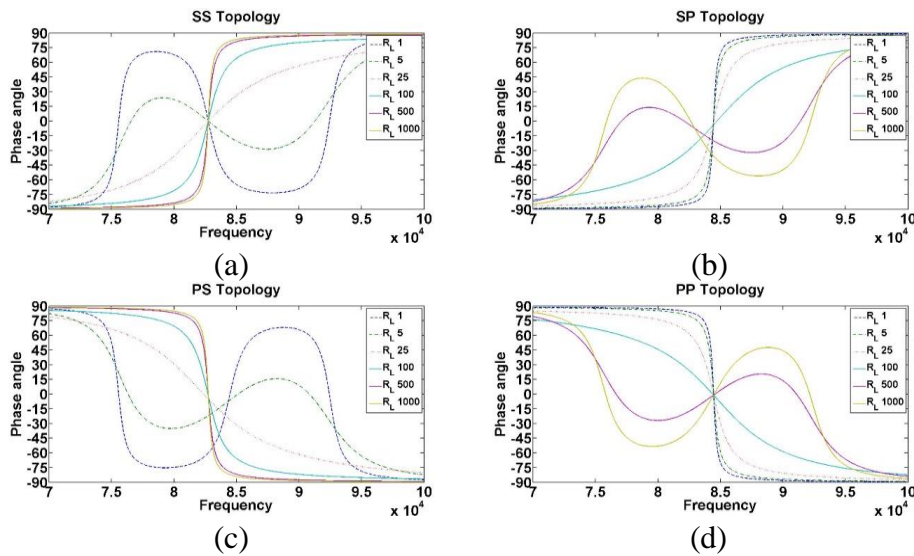


Figure 10 Phase angle-frequency graphs for the (a) SS, (b) SP, (c) PS, and (d) PP topologies.

The SS and SP topologies, which are similar in terms of their transmitter sides, are capacitive below the resonant frequency and inductive above the resonant frequency. However, the PS and PP topologies with parallel compensation on their transmitter sides are inductive below the resonant frequency and capacitive above the resonant frequency.

COMPARISON AND DISCUSSION

Topology selection in WPT systems can vary significantly depending on the load characteristics, transferred power, input source, and many other factors. The efficiency, transmittable input power, load resistance range, equivalent impedance range, and load conditions over and under the resonant frequency for the SS, SP, PS, and PP topologies are compared in Table 2.

Table 2 Comparison between the SS, SP, PS, and PP topologies.

Parameter	SS topology	SP topology	PS topology	PP topology
Efficiency	High	High	High	High
Transmittable power	High	High	Low	Low
Equivalent impedance	Low	Low	High	High
Load resistance	Low	High	High	Low
Power source	Voltage source	Voltage source	Current source	Current source
Under resonant frequency	Capacitive	Capacitive	Inductive	Inductive
Over resonant frequency	Inductive	Inductive	Capacitive	Capacitive

The topology of the receiver side was determined according to the load resistance range for a highly efficient operation. For low-load resistance, such as electric vehicle or mobile phone charging, topologies with series compensation on the receiver side (SS and PS) are preferred. Topologies with parallel compensation on the receiver side (SP and PP) are more suitable for high-load-resistance, low-current, and low-power operations, such as medical implant charging. In applications with a low input voltage, the SS and SP topologies are preferred because their equivalent impedance is low and they can draw a higher current from the input. Although the SS and SP topologies are supplied by a voltage source, the PP and PS topologies cannot be driven directly with voltage sources such as full- or half-bridge inverters owing to the parallel-connected capacitor. If supplied by a voltage source, they draw very high instantaneous currents because there is no inductance to limit the current between the voltage source and the capacitor at the inverter output. Because the switches cannot withstand this high short-circuit current and di/dt , they are likely to be destroyed. Therefore, the PS and PP topologies are supplied by current sources. Because the SS and SP topology circuits operate at resonant frequencies where the equivalent impedance is minimal, they draw more power from the source. Unlike the SS and SP topologies, the equivalent impedance is maximum at the resonant frequency in circuits with the PS and PP topologies; hence, the power drawn from the source is low. When the phase angles with respect to frequency are examined, the SS and SP topologies operate in the capacitive region below the resonance frequency and in the inductive region above the resonance frequency. In contrast, with the PS and PP topologies, operation occurs in the inductive region below the resonant frequency and in the capacitive region above the resonant frequency.

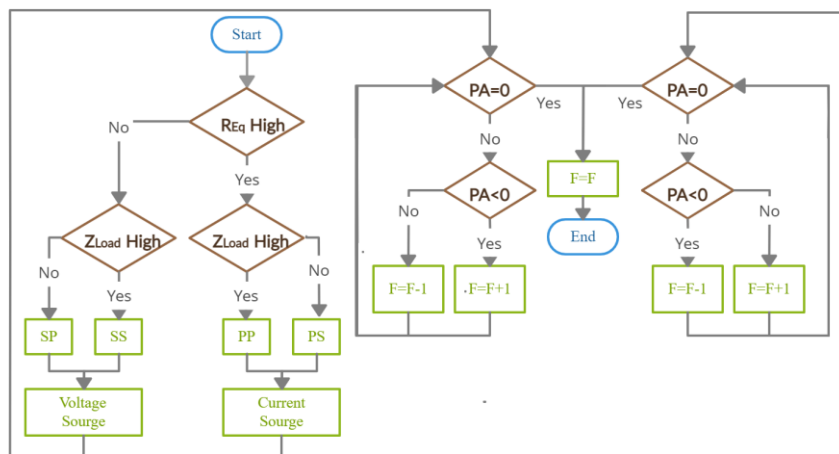


Figure 11 Topology-related input source and resonance frequency determination flowchart.

Figure 11 shows a flowchart for the selection of the appropriate topology, selection of the appropriate source, and determination of the appropriate resonance frequency. PA is the phase angle, and F is the frequency. The selection of suitable circuit parameters for the topology is as important as the determination of the topology itself. Figure 12 shows a flowchart for the determination of the appropriate circuit parameters according to topology.

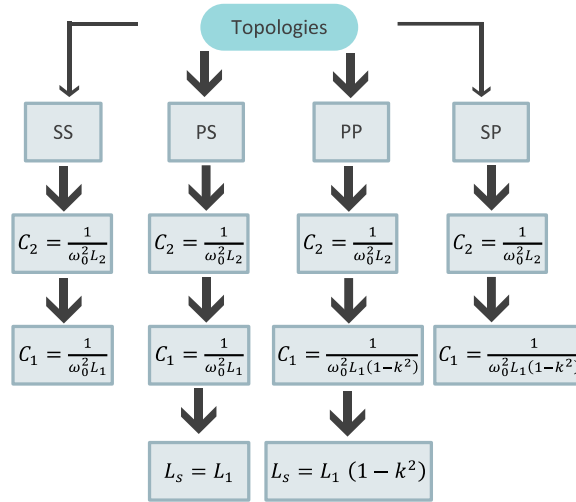


Figure 12. Topology-related circuit parameter determination flowchart.

In PS and PP systems, in which the compensation topology of the transmitter side is parallel, the capacitor cannot be directly connected to the input voltage source. A series inductance L_s is connected between the parallel resonator and either the full-bridge or half-bridge inverter. The inductance value of L_s is determined according to the topology, as shown in Figure 12.

CONCLUSION

This paper presents a simulation-based comparative analysis of four main compensation topologies for two-coil resonant wireless power transfer systems. The system behavior was examined for various parameters, such as efficiency, equivalent impedance, frequency, load resistance, and phase angle. The selection of suitable circuit parameters for a topology is as important as the topology itself. Additionally, a topology selection scheme related to circuit parameters is proposed. A wide range of loads, voltages, and power ranges for topology selection were addressed. Simulations were conducted for the four main topologies under different load conditions. The results clearly indicate that selecting a proper compensation topology for an appropriate load is crucial for the correct operation of the designed system. Analysis results according to frequency under various load conditions show that the variation in efficiency depends on the compensation topology of the receiver side; whereas the topology of the transmitter side only affects the equivalent impedance along with the amount of power drawn from the input. Because the SS and SP topologies operate at resonant frequencies where the equivalent impedance is minimum and a higher current is drawn, in applications with low input voltage, they are preferred and can draw a higher current from the input. Unlike the SS and SP topologies, the equivalent impedance is maximum at the resonance frequency in circuits with the PS and PP topologies; therefore, the transmittable power is lower.

ACKNOWLEDGEMENT

This research was supported by the Yildiz Technical University Scientific Research Projects Coordinatorship grant (FBA-2022-4973).

REFERENCES

- Agcal, A., Ozcira, S., & Bekiroglu, N. 2016.** Wireless power transfer by using magnetically coupled resonators. *Journal of Wireless Power Transfer: Fundamentals and Tech.*, 49-66.
- Aydin, E., Yildiriz, E., & Aydemir, M. T. 2021.** A new semi-analytical approach for self and mutual inductance calculation of hexagonal spiral coil used in wireless power transfer systems. *Electrical Engineering*, 1-10.
- Bekiroglu, N., Agcal, A., & Ozcira, S. 2018.** Validation of wireless power transfer by using 3d representation of magnetically coupled resonators considering peak efficiency. *Journal of Magnetism*, **23**(1): 11-17.
- Gao, P., Tian, Z., Wang, X., Wu, J., & Gui, W. 2018.** Effect of the ratio of radial gap to radius of the coils on the transmission efficiency of wireless power transfer via coupled magnetic resonances. *AIP Advances*, **8**(3), 035020.
- Hasanzadeh, S., & Vaez-Zadeh, S. 2015.** A review of contactless electrical power transfer: Applications, challenges and future trends. *Automatika*, **56**(3): 367-378.
- Heidarian, M., & Burgess, S. J. 2020.** A design technique for optimizing resonant coils and the energy transfer of inductive links. *IEEE Transactions on Microwave Theory and Techniques*, **69**(1): 399-408.
- Keerthi, K. S., Ilango, K., & Manjula, G. N. 2018.** Study of midfield wireless power transfer for implantable medical devices. *2nd International Conference on Biomedical Engineering (IBIOMED)*. 44-47
- Nataraj, C., Khan, S., Habaebi, M. H., & Muthalif, A. G. 2018.** General Analysis of Resonance Coupled WPT Using Inductive Coils. *Tehnički Vjesnik*, **25**(3): 720-726.
- Ravikiran, V., & Keshri, R. K. 2017.** Comparative evaluation of SS and PS topologies for wireless charging of electrical vehicles. *43rd Annual Conference of the IEEE Industrial Electronics Society*. 5324-5329.
- Tang, W., & Cheng, Z. 2020.** A Real-Time Tracking Algorithm for 3D Wireless Maximum Power Transfer to a Moving Device. *IEEE PELS Workshop on Emerging Technologies: Wireless Power Transfer*. pp. 27-34.
- Waters, B. H., Mahoney, B. J., Lee G. and Smith, J. R. 2014.** Optimal coil size ratios for wireless power transfer applications. *IEEE 2014 International Symposium on Circuits and Systems (ISCAS)*, pp. 2045-2048.
- Zavřel, M., & Kindl, V. 2018.** Comparison of Various Configuration of Wireless Power Transfer System. *Transactions on Electrical Engineering*, **7**(2): 32-36.
- Zeng, R., Galigekere, V. P., Onar, O. C., & Ozpineci, B. 2021.** Grid Integration and Impact Analysis of High-Power Dynamic Wireless Charging System in Distribution Network. *IEEE Access*, **9**: 6746-6755.